Exploiting the spatial extension of impurity for regulation of a few electrical properties of GaAs quantum dot: Role of noise

B. Bhakti and M. Ghosh

Department of Chemistry, Physical Chemistry Section, Visva-Bharati University, Santiniketan, Birbhum-731235, West Bengal, India.
e-mails: pcmg77@gmail.com; manasghosh.chem@visva-bharati.ac.in

Received 24 November 2024; accepted 20 February 2025

The study uncovers the role of delicate interplay between *spatial dispersion of impurity* and *Gaussian white noise* on a few *electrical* properties of the *doped* GaAs *quantum dot (QD)*. The electrical properties involve *static dipole polarizability (SDP)*, *dynamic dipole polarizability (DDP)*, *quadrupole oscillator strength (QOS)* and *static quadrupole polarizability (SQP)*. The interplay between noise and the impurity spread depends on the pathway (additive/multiplicative) by which noise is applied. It has been found that, a gradual modulation of impurity spread, in conjunction with the mode of entry of noise, can effectively regulate the above electrical properties.

Keywords: Quantum dot; impurity spread; Gaussian white noise; electrical properties.

DOI: https://doi.org/10.31349/RevMexFis.71.041601

1. Introduction

All low-dimensional nanostructures such as *quantum wells (QWLs)*, *quantum wires (QWRs)*, *quantum well wires (QWWs)* and *quantum dots (QDs)* almost invariably contain impurities. The presence of impurities significantly influences the various physical properties of semiconductor nanostructures. Specifically, doping of shallow impurities to these nanostructures is characterized by remarkable changes in their electric, magnetic, thermodynamic, transport and optical properties. Utilizing the capability of the modern fabrication techniques to dope impurities in a controlled way, the physical properties mentioned above can also be tuned in a desired manner thereby providing important insights into manufacture of advanced quantum devices. In consequence, a plethora of research works have been dedicated towards understanding the impurity effects in these nanostructures [1–23], giving sufficient importance on their *Nonlinear optical (NLO)* properties [1, 3–5, 7, 8, 10, 16–19, 24–53]. Among the other important works on the NLO properties, a few deserve special mention. Restrepo et al studied second and third harmonic generation associated to infrared transitions in a Morse quantum well under applied electric and magnetic fields [54]. Yesilgul et al examined the linear and nonlinear optical properties in an asymmetric double quantum well under intense laser field [55]. Duque et al explored the intense laser effects on donor impurity in a cylindrical single and vertically coupled quantum dots under combined effects of hydrostatic pressure and applied electric field [56].

The *spatial spread of impurity* directly regulates the QD-impurity interaction as it governs the proximity of the electron to the impurity location. Therefore, a change in the spatial dissemination of impurity brings about a consequent change in the degree of QD-impurity overlap and hence in the confinement potential. As a natural outcome, the energy levels and the various matrix elements of the QD are profoundly altered leading to noticeable change in the various physical properties.

External electric field (F) bears important implications in the physics of low-dimensional nanostructures. The electric field causes a shift of the energy states of these systems (*Stark shift*) thereby changing the energy spectra. Such change is accompanied by polarization of the carrier distribution and consequent loss in the symmetry of the system. As a result, it becomes possible to clearly understand the features of the carrier distribution.

Dipole polarizabilities (DPs) of a system indicates its lowest-order response to an external electric field that results into the distortion of electron cloud [57, 58]. In presence of the external electric field the center of negative charge distribution is shifted and induces an electric dipole moment. Dipole polarizability links the dipole moment, thus generated, to the electric field strength. For a time-independent electric field we call it the *static dipole polarizability (SDP)*. It is a linear response property, mathematically defined as the second differential coefficient of total energy with respect to an external homogeneous electric field. Physically, SDP acts as an indicator of changes in the charge distribution, achieved through the distortion of the electronic density because of the static electric field. SDP depends on the attributes of the wave function of the system [59, 60]. The studies of DPs bear immense significance in understanding the pressure effects on the system, various interactions operating inside the system, scattering phenomenon, optical properties, dielectric constant, ion mobility in gas, the van-der-Waals constant, the long range electron-atom interaction etc. [58, 61]. On the other hand, if the system is subjected to a time-dependent radiation field of frequency (ν), one obtains *dynamic dipole polarizability (DDP)* [59, 60, 62–64].

Quadrupole oscillator strength (QOS) is a highly important quantity for understanding the optical properties that are connected with the electronic quadrupole allowed transitions. A large value of QOS points to high quadrupole moment expectation values and exhibition of substantially large NLO response. The QOS involves the quadrupole moment operator ($\propto r^2$) [65, 66]. Naturally, a few studies have been devoted to exploring the QOS in low-dimensional nanostructures [67–69].

Static quadrupole polarizability (SQP) generates owing to the quadrupole moment induced by an external electric field gradient [67]. SQP plays anchoring role in the calculation of the ionic contribution to the electric field gradient in solids [65, 70, 71]. The work of Yakar et al explores SQP of spherical QD [67].

It now appears relevant to elucidate the focus and the novelty of the current work. The work conducts a scrupulous monitoring of how a change in the *spatial width of impurity* can tailor a few *electrical properties* of GaAs QD under the active presence of *noise*. Since both impurity and noise are known to affect the properties of the low-dimensional nanostructures, simultaneous presence of both of them would undoubtedly be very interesting. Now, it would be the interplay between them which would be the governing factor. A gradual change in the spatial width of the dopant causes a parallel change in the said interplay paving the way for harnessing the electrical properties in delicate ways.

Specifically, present investigation explores the GaAs QD that has been doped with *Gaussian impurity* under the simultaneous presence of *Gaussian white noise*. The QD confinement involves lateral parabolic potential (which spatially restricts the electronic motion to the $x-y$ surface), a vertical magnetic field, the impurity potential and noise. Inclusion of noise invites greater complexity that stems from its pathway of application (additive/multiplicative). The study explores *SDP*, *DDP*, *QOS* and *SQP* as the electrical properties of concern and analyzes their modulations under the joint influence of changing spatial spread of impurity and noise.

2. Method

Under the effective mass approximation, the QD Hamiltonian consisting of the lateral parabolic confinement, impurity, vertical magnetic field, lateral electric field and noise turns out to be

$$H_0 = H_0' + V_{imp} + |e|F(x+y) + \xi(x,y). \tag{1}$$

The dopant-free Hamiltonian viz. H_0' consists of the basic parabolic confinement [$\frac{1}{2}m^*\omega_0^2(x^2+y^2)$] and the effect of the magnetic field:

$$H_0' = \frac{1}{2m^*}\left[-i\hbar\nabla + \frac{\mathbf{e}}{\mathbf{c}}\mathbf{A}\right]^2 + \frac{1}{2}m^*\omega_0^2(x^2+y^2), \tag{2}$$

with ω_0, m^* and $\mathbf{A}$ denote the confinement frequency, the electronic effective mass, and the vector potential [given by $A = (By, 0, 0)$ in Landau gauge where B is the magnetic field strength]. H_0' then appears to be

$$H_0' = -\frac{\hbar^2}{2m^*}\left(\frac{\partial^2}{\partial x^2} + \frac{\partial^2}{\partial y^2}\right) + \frac{1}{2}m^*\omega_0^2x^2 + \frac{1}{2}m^*\Omega^2y^2 - i\hbar\omega_c y\frac{\partial}{\partial x}, \tag{3}$$

where ω_c and $\Omega(=\sqrt{\omega_0^2+\omega_c^2})$ are the cyclotron frequency and the gross confinement frequency in the y-direction. Thus, the contribution of the magnetic field strength is contained within ω_c.

The three dopant parameters, namely, the dopant potential strength (V_0), the dopant location (x_0, y_0) and the spatial extension of the dopant ($\gamma^{-1/2}$) constitute the Gaussian impurity potential (V_{imp}) [cf. Eq. (1)] which can be algebraically expressed as:

$$V_{imp} = V_0\, e^{-\gamma\left[(x-x_0)^2+(y-y_0)^2\right]}. \tag{4}$$

A large (small) γ value suggests spatially squeezed (expanded) impurity potential.

The term $|e|F(x+y)$ [cf. Eq. (1)] represents the contribution coming from the static electric field of magnitude F and operating along x and y axes.

The function $\xi(x,y)$ [cf. Eq. (1)] carries the features of *zero-mean* and *spatial δ-correlation* and stands for the Gaussian white noise. $g(x,y)$ is a second function, associated with $\xi(x,y)$, and gives a mathematical description of the above traits as outlined below:

$$\langle g(x,y)\rangle = 0, \tag{5}$$

and

$$\langle g(x,y)g(x',y')\rangle = 2\zeta\delta\left[(x,y)-(x',y')\right], \tag{6}$$

respectively, with noise strength ζ. Box-Muller algorithm produces $g(x,y)$ obeying Gaussian distribution. The highly fluctuating term $g(x,y)$ is called *white noise* because of a flat spectrum in space, similar to the white light. Spatially δ-correlated Gaussian white noise suggests a signal whose components consist of series of spatially uncorrelated random disturbances. This makes noise absolutely random in nature with zero memory effect. In other words, noise at any given spatial location remains unperturbed by its magnitude at any other locations. The noises strength ζ defines the intensity of fluctuation. The zero-mean guarantees that, each sample/component belonging to the signal maintains a Gaussian distribution with zero mean *i.e.* the disturbance is uniformly as well as randomly spread over space. Box-Muller algorithm produces random deviates having a normal (Gaussian) distribution. It is a random number sampling method for producing pairs of independent, standard, normally distributed (zero mean) random numbers, from a source of uniformly distributed random numbers [72]. One may consult pages 279-280 of the reference [72] where the algorithm (subroutine) is given.

The pattern of linkage between $\xi(x,y)$ and $g(x,y)$ determines the diverse ways of applying Gaussian white noise to the QD, viz. *Additive white noise* and *multiplicative white noise* which read

$$\xi(x,y) = \lambda_1 g(x,y), \quad \text{for additive white noise (NSADD)}, \tag{7}$$

and

$$\xi(x,y) = \lambda_2 g(x,y)(x+y), \quad \text{for multiplicative white noise (NSMLT)}, \tag{8}$$

where λ_1 and λ_2 are the two constants. These constants take care of the influence of surrounding environment for additive and multiplicative noise, respectively. In effect, the magnitude (*i.e.* the impact) of these λ-s are absorbed within the noise strength ζ. Therefore, no separate values of these λ-s are needed. A change in the noise strength becomes actually meaningful from a physical perspective.

Linear variational principle has now been invoked for an approximate solution to the time-independent Schrödinger equation. For this purpose, the ordinary product of the harmonic oscillator eigenfunctions has been chosen as the trial function $\psi_k(x,y)$. The normalized eigenvectors and the energy eigenvalues can thus be subsequently generated.

SDP, for confined systems, can be given by [59]

$$\alpha_D = 2e^2 \sum_{j=1} \frac{|\langle\psi_j^{(0)}|x+y|\psi_0^{(0)}\rangle|^2}{E_j^{(0)} - E_0^{(0)}}, \tag{9}$$

where, e, $\psi_j^{(0)}$ and $\psi_0^{(0)}$ are the electronic charge and the $|j\rangle$-th and $|0\rangle$-th eigenstates in absence of the electric field, respectively. $E_j^{(0)}$ and $E_0^{(0)}$ are the associated energies. Present inspection takes into account the first five eigenstates (*i.e.* $|j\rangle = |1\rangle$ to $|5\rangle$) in the above summation. This is due to the fact that the transition dipole moment values among these states are much larger than other states. Consideration of more terms in the above summation does not possess any meaningful significance but unnecessarily hikes the computational labour.

While considering DDP, the QD is exposed to an electric field of magnitude F which oscillates with a frequency ν. The QD experiences an electrically introduced perturbation which is a function of both frequency and time and is given by [60, 62]

$$V(\nu,t) = F\left[exp(-2\pi i\nu t) + exp(2\pi i\nu t)\right], \tag{10}$$

and DDP is given by the following expression [59]

$$\alpha_D(\nu) = \sum_{j=1} \frac{f_{j0}}{\left(E_j^{(0)} - E_0^{(0)}\right)^2 - (h\nu)^2}, \tag{11}$$

where $h\nu$ and f_{j0} are the photon energy and the oscillator strength corresponding to the $|0\rangle \rightarrow |j\rangle$ transitions. The oscillator strength for the dipole allowed transitions can be expressed as [59]:

$$f_{j0} = \frac{2}{3}\Delta E_{j0}|\langle\psi_j^{(0)}|x+y|\psi_0^{(0)}\rangle|^2,$$

where, $\psi_j^{(0)}$ and $\psi_0^{(0)}$ are the $|j\rangle$-th and $|0\rangle$-th eigenstates in absence of the electric field, and $E_j^{(0)}$ and $E_0^{(0)}$ are the associated energies. Current study computes DDP for the $|0\rangle \rightarrow |1\rangle$ transition owing to its substantially large value of transition dipole moment. DDP possesses *singular points* at $h\nu = E_1^{(0)} - E_0^{(0)}$ which are responsible for its *sign-inversion*.

Following the absorption or emission of photons for the transition between the states $|i\rangle$ and $|f\rangle$, the QOS $[P^{(2)}]$ can be written as [67]

$$P^{(2)} = 2\,|\langle f|x^2+y^2|i\rangle|^2\,(E_f - E_i)\,, \tag{12}$$

where E_i and E_f being the initial and final state energies, respectively.

Finally, SQP can be expressed as [67]

$$\alpha_{sqp} = \sum_{f>i} \frac{P^{(2)}}{(E_f - E_i)^2}, \tag{13}$$

where $P^{(2)}$ is the QOS as outlined before.

3. Results and discussion

In general, for the doped GaAs QD, the various physical parameters take on following values: $m^* = 0.067m_0$, where m_0 is the vacuum electron mass, $\varepsilon = 12.4$ is the dielectric constant, $\hbar\omega_0 = 100.0$ meV, $B = 5.0$ T, $F = 100$ kV/cm, $V_0 = 200.0$ meV, $r_0 = 0.0$ nm and $\zeta = 1.0 \times 10^{-4}$, respectively. The effects of the constants λ_1 and λ_2 that appear in Eq. (7) and Eq. (8) are absorbed inside the noise strength ζ. The ζ value is so chosen that the noise contribution remains overall rather small so that the numerical stability is not compromise.

3.1. Static dipole polarizability

Figure 1 displays the static dipole polarizability (SDP) plots as a function of the impurity spread without noise and with NSADD and NSMLT, respectively. The plots reveal steady enhancement of SDP with increase in impurity spread, both in presence and absence of noise.

An increase in the spatial spread of impurity reduces the system confinement. In consequence, the system gradually gets expanded and SDP increases [59, 61, 63]. Moreover, presence of NSADD (NSMLT) raises (lowers) SDP with respect to the noise-free ambience over a wide range of impurity spread. This suggests that applied NSADD (NSMLT) enhances (depletes) the expansive nature of the system from that under the state without noise. Thus, the SDP profiles quantitatively depend on the noise mode. It can be further

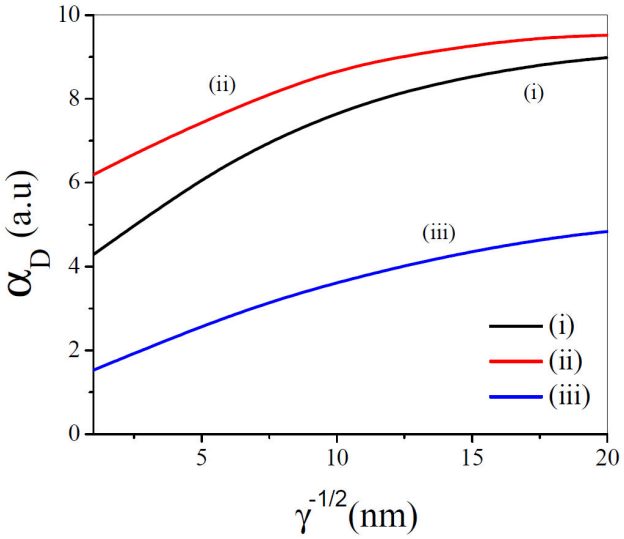

FIGURE 1. SDP plots against impurity spatial stretch ($\gamma^{-1/2}$): (i) without noise, (ii) under NSADD and (iii) under NSMLT.

noted that, with increase in the spatial spread of impurity, the SDP function seems to take on an approximately constant (horizontal) behavior. This may be due to the fact that, in the regime of very large value of impurity spread, the system's expansion settles to some sort of steady value. And no further expansion of the system occurs even if the spatial dispersion of the impurity is enhanced further. This is reflected through approximately constant values of the SDP in the large impurity spread domain.

3.2. Dynamic dipole polarizability

Figures 2a)-2c) show the dynamic dipole polarizability (DDP) profiles against the oscillation frequency (ν) for different values of impurity spread, with and without noise. It comes out that, regardless of presence of noise, for a given value of impurity spread an increase in the incoming frequency enhances the DDP [59, 64]. Moreover, with increase in the impurity spread, the singular point makes a shift towards the lower photon energy. Furthermore, it can also be noticed that DDP takes on positive (negative) values as the incident photon frequency lies to the left (right) of the singular point. This happens since the incoming photon frequency has been varied in the immediate vicinity of $\Delta E_{01} = E_1^{(0)} - E_0^{(0)}$

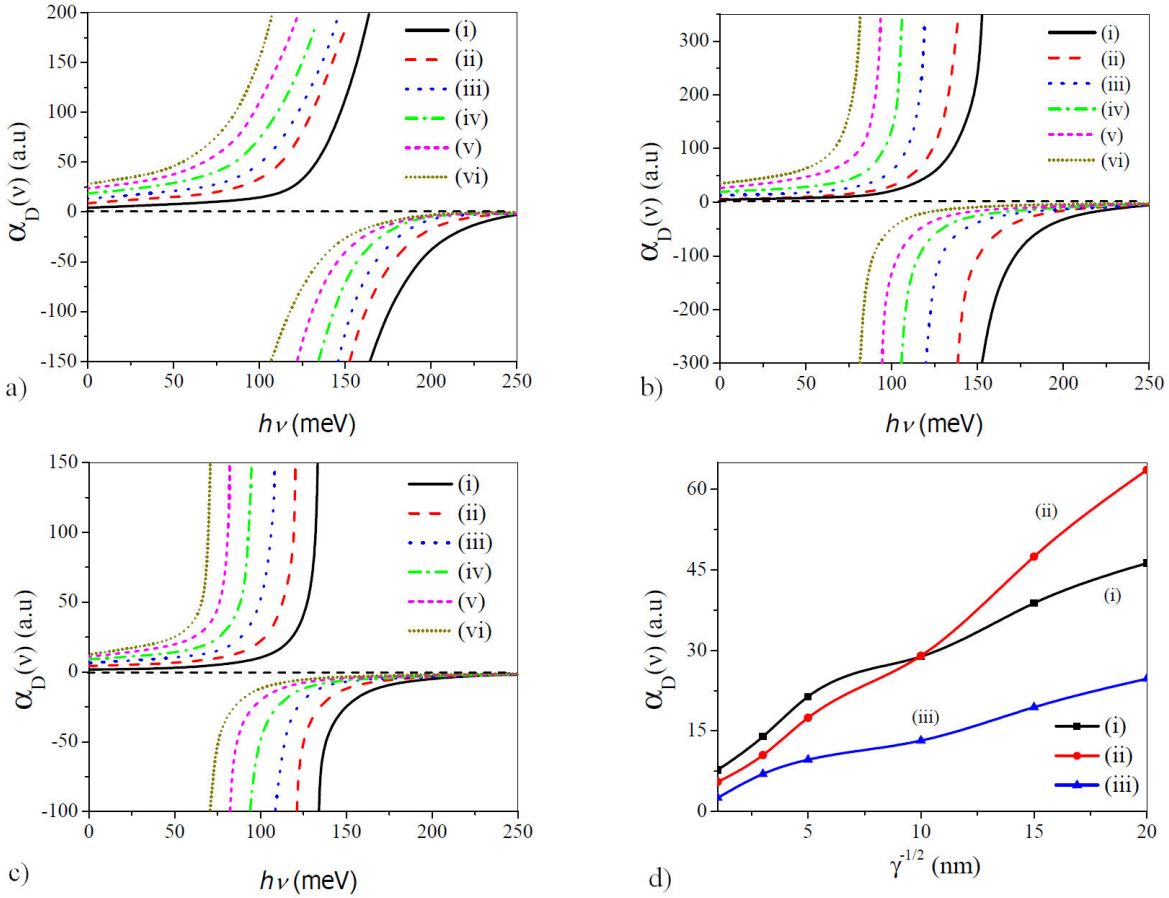

FIGURE 2. DDP diagrams against $h\nu$ for different values of impurity spatial stretch ($\gamma^{-1/2}$): (i) 1 nm, (ii) 3 nm, (iii) 5 nm, (iv) 10 nm, (v) 15 nm and (vi) 20 nm: a) without noise, b) with NSADD and c) with NSMLT. d) Profiles of DDP vs $\gamma^{-1/2}$ at $h\nu = 50$ meV: (i) without noise, (ii) with NSADD and (iii) with NSMLT.

interval. The frequency range has been chosen looking at the $|0\rangle \rightarrow |1\rangle$ transition which makes the most substantial contribution in the summation of Eq. (11).

Figure 2d) exhibits the DDP profiles as a function of the impurity stretch at a given value of the impinging photon energy of $h\nu = 50$ meV. The plots reveal that, irrespective of presence of noise, the DDP steadily enhances following the enhancement of impurity spread. The finding suggests a fall of the effective confinement of the system with increase in the impurity stretch. The reduced confinement decreases the energy interval between the eigenstates leading to enhanced oscillator strength and thereby augments the DDP [59, 64]. Quantitatively, DDP registers lowest value in presence of NSMLT. However, the magnitudes of DDP without noise and in presence of NSADD make a crossover in the vicinity of $\gamma^{-1/2} \sim 10$ nm. The DDP exhibits higher values without noise than in presence of NSADD inside the regime $\gamma^{-1/2} < 10$ nm whereas the situation exactly reverses as the impurity spread exceeds the above value. Thus, once again, the applied NSMLT happens to enhance the system confinement from the noise-free ambience. However, the modification of system confinement (with respect to the noise-free environment) by NSADD noticeably depends on the extent of spatial spread of impurity. Whereas for low-to-medium impurity spread ($\gamma^{-1/2} < 10$ nm) NSADD increases the system confinement over the noise-free state, it does just the reverse within high impurity spread regime ($\gamma^{-1/2} > 10$ nm).

The overall magnitude of DDP depends on the relative dominance of the factors such as the energy separation between the eigenstates, the relevant oscillator strength and the incoming photon frequency. A varying impurity spread, presence of noise and the mode of application of noise, in combination, affect the said energy intervals and the oscillator strength and therefore design the features of the DDP profiles. The study makes it conspicuous that DDP of doped QD can be regulated through the effective manipulation of the confinement (achieved through the variation of impurity spread and applied noise in a given mode) as well as by tuning the incoming photon frequency.

It needs to be mentioned that, both SDP and DDP profiles manifest qualitatively similar features as a function of the electric field strength (F) as observed with impurity spread. This is because, quite similar to the impurity spread, an increase in F also diminishes the overall confinement of the system. We, therefore, refrain from elaborating the profiles of SDP and DDP against F for the brevity of the manuscript.

3.3. Quadrupole oscillator strength

Figure 3 delineates the quadrupole oscillator strength (QOS) profiles following the variation of spatial stretch of impurity, both including and excluding noise. Without noise and in presence of NSMLT the profiles display a regularly decreasing trend as the spatial stretch enhances. In presence of NSADD, the decreasing trend persists but now it consists of a minimum around $\gamma^{-1/2} \sim 10$ nm. QOS is governed by two

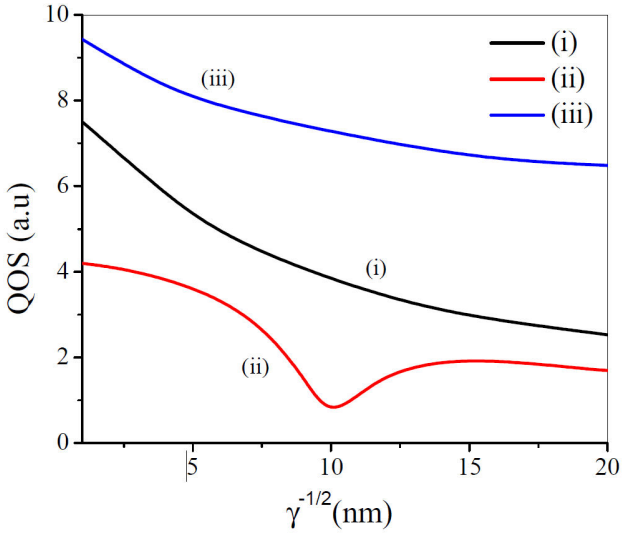

FIGURE 3. QOS plots against impurity spatial stretch ($\gamma^{-1/2}$): (i) excluding noise, (ii) including NSADD and (iii) including NSMLT.

factors, namely, the quadrupole matrix element $|\langle f|x^2 + y^2|i\rangle|$ and the energy interval $(E_f - E_i)$ between the eigenstates. In the present study, the QOS profiles plotted against impurity spread show noticeable dependence on the noise mode. The steady decline of QOS under noise-free state and in presence of NSMLT can take place if both the above factors decrease with increase in $\gamma^{-1/2}$. Alternatively, it is also possible that one of the above factors increases with increase in the impurity stretch while the other factor decreases. Now, if the decreasing factor dominates over the increasing factor then there will be an overall drop in the QOS as spatial spread of impurity increases. Emergence of minimization in QOS in presence of NSADD indicates kind of opposing behaviour between the above two factors and a shift in the relative dominance between them in the vicinity of $\gamma^{-1/2} \sim 10$ nm. Thus, the features of the QOS profiles depend on the presence/absence of noise and also on the noise mode. Furthermore, over a wide range of impurity stretch, applied NSADD (NSMLT) lowers (raises) the QOS from the noise-free value.

3.4. Static quadrupole polarizability

Figure 4 describes the static quadrupole polarizability (SQP) profiles pursuing the change of spatial dispersion of impurity, both considering and ignoring noise. In absence of noise and under NSADD the SQP plots manifest distinct maximization in the neighborhood of $\gamma^{-1/2} \sim 5$ nm and $\gamma^{-1/2} \sim 8.5$ nm, respectively. However, in presence of NSMLT, the SQP depicts a nearly steady behaviour consisting of minor fluctuations with variation of impurity spread. The magnitude of SQP is guided by the quadrupole oscillator strength $P^{(2)}$ and the energy separation $(E_f - E_i)$ between the eigenstates. However, the $P^{(2)}$ term itself depends on the energy difference $(E_f - E_i)$ and also on the quadrupole matrix element $|M_{if}^{(2)}| = |\langle f|x^2 + y^2|i\rangle|$. The SQP could increase (with

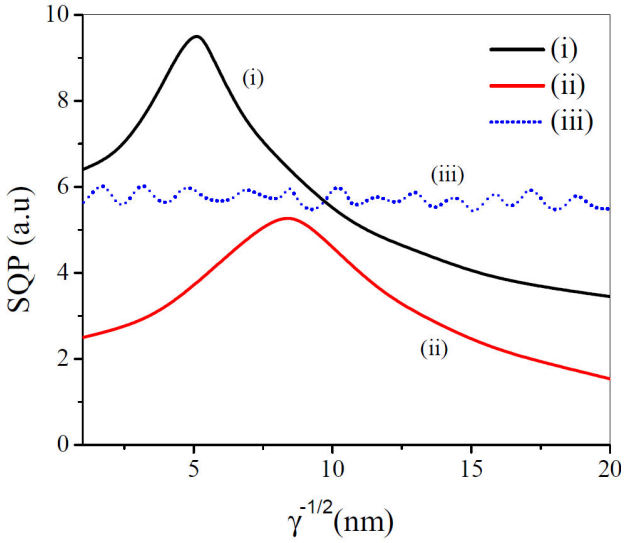

FIGURE 4. SQP curves as a function of spatial dispersion of impurity ($\gamma^{-1/2}$): (i) ignoring noise, (ii) considering NSADD and (iii) considering NSMLT.

variation of the impurity spread) if $P^{(2)}$ increases associated with a fall of energy interval. However, since $P^{(2)}$ itself contains the energy separation term, a fall of the said separation will also lower $P^{(2)}$. This needs to be noted that, whereas SQP depends inversely on the square of energy separation, $P^{(2)}$ has a linear dependence on energy difference. Thus, it will be the resultant impact of $P^{(2)}$, the energy gap and $|M_{if}^{(2)}|$ which ultimately shapes the enhancement of SQP. By virtue of similar argument the decline of SQP can also be envisaged. Emergence of maximization in absence of noise and under NSADD indicates a competitive behavior between the above parameters and accompanying shift in the relative dominance among them as the impurity spread disperses over a range. In presence of NSMLT, a steady SQP indicates kind of compromise among these diverse factors over a wide range of impurity stretch.

Physically, rise and fall of SQP indicate greater spreading and squeezing of wave function [67] due to reduced and enhanced effective confinement of the system, respectively, as the impurity spread varies over a range under different conditions. On the other hand, a steady SQP suggests a somewhat fixed spread of wave function owing to sort of stable effective confinement potential. In this case, even a change in the spatial stretch of impurity fails to appreciably modify the effective confinement of the system. Although, qualitatively the SQP profiles appear similar without noise and under NSADD, they differ in magnitude and location of emergence of maxima. The difference arises due to alteration of the effective confinement by the presence of NSADD with respect to the situation without noise. Applied NSADD seems to enhance the confinement and reduce the stretch of wave functions leading to a drop in SQP from the noise-free state. The similarity in the SQP profiles without noise and in presence of NSADD stems from the fact that, by virtue of the very nature of coupling with the system, NSADD perturbs the noise-free system usually in rather small amount. On the other hand, NSMLT makes a strong coupling with the system and usually causes large deviation of system's properties from the noise-free state. In the present enquiry, presence of NSMLT produces steady SQP over the entire range of impurity stretch comprising of frivolous undulations. Thus, it can be argued that the presence of NSMLT affects the confinement in such a way so that a continuous balance persists among the various factors that govern SQP. In consequence, the overlap between the eigenstates becomes quite stable over the entire range of impurity stretch leading to steady SQP.

4. Conclusion

The interplay between the spatial dispersion of Gaussian impurity and Gaussian white noise delicately regulates the electrical properties of GaAs QD. The electrical properties considered are SDP, DDP, QOS and SQP. Gradual change in impurity spread, coupled with the pathway of application of noise, can regulate the said electrical properties. Under all conditions, a gradual increase in impurity spread enhances SDP and DDP. Without noise and in presence of multiplicative noise, QOS monotonically falls with increase in impurity stretch, whereas, in presence of additive noise, the QOS minimizes at an impurity spread of $\sim$ 10 nm. The SQP, on the other hand, manifests maximization at impurity spread of $\sim$ 5 nm and $\sim$ 8.5 nm under noise-free atmosphere and under additive noise, respectively. However, application of multiplicative noise leads to a steady SQP over a wide range of impurity stretch.

It needs to be mentioned that the present study considers only on-center dopants *i.e.* the impurity position has been kept fixed at the origin. However, the impurity may be placed at centers away from origin (the off-center impurities). For off-center impurities, because of the enhanced separation between QD confinement center and the dopant, it is expected that the profiles of the electrical properties would be quantitatively affected. However, no major qualitative change can be expected. The study with off-center impurities will be an entirely separate one and we hope to explore this in near future.

Acknowledgements

The authors B. B. and M. G. thank DST-FIST (Govt. of India) and UGC-SAP (Govt. of India) for support.

Author contributions

Both the authors contributed substantially to the paper. MG originated the topic of the research. MG did all the analytical and numerical calculations besides writing the draft of the paper. MG also reviewed the analytical calculations and revised the initial draft of the paper. BB took active part in computational aspects and overall monitoring of the work.

Data availability statement

It is hereby stated that the current manuscript has no associated data or the data will not be deposited.

Conflict of interest statement

The authors declare that they have no conflict of interest.

1. M. G. Barseghyan, V. N. Mughnetsyan, L. M. Pérez, A. A. Kirakosyan, and D. Laroze, Effect of the impurity on the Aharonov-Bohm oscillations and the intraband absorption in $GaAs/Ga_{1-x}Al_xAs$ quantum ring under intense THz laser field, *Physica E* **111** (2019) 91, https://doi.org/10.1016/j.physe.2019.03.003.
2. L. M. Pérez, N. Aghoutane, D. Laroze, P. Díaz, M. El-Yadri, and El M. Feddi, Unveiling the role of donor impurity position on the electronic properties in strained type I and type II core/shell quantum dots under magnetic field, *Materials* **16** (2023) 6535, https://doi.org/10.3390/ma16196535.
3. G. A. Mantashian, N. A. Zaqaryan, P. A. Mantashyan, H. A. Sarkisyan, S. Baskoutas, and D. B. Hayrapetyan, Linear and nonlinear optical absorption of *Cdse/Cds* core/shell quantum dots in the presence of donor impurity, *Atoms* **9** (2021) 75, https://doi.org/10.3390/atoms9040075.
4. R. G. Toscano-Negrette, J. C. León-González, J. A. Vinasco, A. L. Morales, F. Koc, A. E. Kavruk, M. Sahin, M. E. Mora-Ramos, J. Sierra-Ortega, J. C. Martínez-Orozco, R. L. Restrepo, and C. A. Duque, Optical properties in a ZnS/CdS/ZnS core/shell/shell spherical quantum dot: Electric and magnetic field and donor impurity effects, *Nanomaterials* **13** (2023) 550, https://doi.org/10.3390/nano13030550.
5. H. R. Rastegar Sedehi, R. Khordad, and H. Bahramiyan, Optical properties and diamagnetic susceptibility of a hexagonal quantum dot: impurity effect, *Optical and Quantum Electron.* **53** (2021) 264, https://doi.org/10.1007/s11082-021-02927-7.
6. R. Khordad, H. R. Rastegar Sedehi, and H. Bahramiyan, Effects of impurity and cross-sectional shape on entropy of quantum wires, *J. Computational Electron.* **17** (2018) 551, https://doi.org/10.1007/s10825-018-1133-9.
7. D. Bejan and C. Stan, Impurity and geometry effects on the optical rectification spectra of quasi-elliptical double quantum rings, *Physica E* **147** (2023) 115598, https://doi.org/10.1016/j.physe.2022.115598.
8. D. Bejan and C. Stan, Electron spin and donor impurity effects on the absorption spectra of pseudo-elliptic quantum rings under magnetic field, *Philosophical Magazine* **101** (2021) 1871, https://doi.org/10.1080/14786435.2021.1939900.
9. R. En-nadir, H. El-ghazi, M. Tihtih, W. Belaid, S. E. Zaki, I. Maouhoubi, and I. Zorkani, Analyzing the combined influences of external electric field, impurity-location, in-content, and QW's number on donor-impurity binding energy in multiple quantum wells with finite squared potential, *Optical and Quantum Electron.* **55** (2023) 597, https://doi.org/10.1007/s11082-023-04893-8.
10. A. Fakkahi, M. Kirak, and A. Sali, Effect of impurity position and electric field on the optical absorption coefficients and oscillator strength in spherical multilayer quantum dot, *Eur. Phys. J. Plus* **137** (2022) 1, https://doi.org/10.1140/epjp/s13360-022-03279-1.
11. Md. K. Elsaid, A. Shaer, E. Hjaz, and M. H. Yahya, Impurity effects on the magnetization and magnetic susceptibility of an electron confined in a quantum ring under the presence of an external magnetic field, *Chinese J. Phys.* **64** (2020) 9, https://doi.org/10.1016/j.cjph.2020.01.002.
12. A. Yaseen, A. Shaer, and Md. K. ElSaid, The magnetic properties of *GaAs* parabolic quantum dot in the presence of donor impurity, magnetic and electric fields, *Chinese J. Phys.* **60** (2019) 598, https://doi.org/10.1016/j.cjph.2019.05.031.
13. O. Akankan, I. Erdogan, A. I. Mese, E. Cicek, and H. Akbas, The effects of geometrical shape and impurity position on the self-polarization of a donor impurity in an infinite GaAs/AlAs tetragonal quantum dot, *Indian J. Phys.* **95** (2021) 1341, https://doi.org/10.1007/s12648-020-01813-4.
14. A. I. Mese, E. Cicek, I. Erdogan, O. Akankan, and H. Akbas, The effect of dielectric constant on binding energy and impurity self-polarization in a GaAs-$Ga_{1-x}Al_xAs$ spherical quantum dot, *Indian J. Phys.* **91** (2017) 263, https://doi.org/10.1007/s12648-016-0921-y.
15. M. Tshipa and G. K. Nkoni, Donor binding energies in a spherical core-shell quantum dot: parabolic and shifted parabolic shell potentials, *Indian J. Phys.* **94** (2020) 633, https://doi.org/10.1007/s12648-019-01513-8.
16. S. Ghajarpour-Nobandegani and M. J. Karimi, Effects of hydrogenic impurity and external fields on the optical absorption in a ring-shaped elliptical quantum dot, *Optical Mater.* **82** (2018) 75, https://doi.org/10.1016/j.optmat.2018.05.045.
17. M. K. Bahar and P. Başer, Combined effects of thermodynamic factors and external fields for nonlinear optical processes of deformed Mathieu quantum dot containing central impurity, *Phys. Lett. A* **483** (2023) 129046, https://doi.org/10.1016/j.physleta.2023.129046.
18. M. Chnafi, O. Mommadi, A. El Moussaouy, S. Chouef, R. Boussetta, M. Hbibi, C. A. Duque, and F. Falyouni, Optoelectronic properties of an off-center donor atom in a wedge-shaped quantum dot under the combined effect of electric and magnetic fields, *Optik* **310** (2024) 171881, https://doi.org/10.1016/j.ijleo.2024.171881.
19. S. Chouef, O. Mommadi, R. Boussetta, M. Hbibi, A. El Moussaouy, M. Şahin, F. Falyouni, and C. A. Duque, Effects of surface curvature and electric field on electronic and optical properties of an off-center hydrogenic donor impurity in 2D

nanostructures, *Eur. Phys. J. Plus* **139** (2024) 381, https://doi.org/10.1140/epjp/s13360-024-05164-5.

20. R. En-nadir, H. El-Ghazi, M. Tihtih, S. E. Zaki, W. Belaid, I. Maouhoubi, and I. Zorkani, Exploring the electronic properties of shallow donor impurities in modified ⋂-shaped potential: Effects of applied electric field, parabolicity, compositions, and thickness, *Eur. Phys. J. B* **96** (2023) 78, https://doi.org/10.1140/epjb/s10051-023-00539-6.
21. G. L. García and L. Meza-Montes, Effect of magnetic field and impurities in *InAs/GaAs* and *GaN/AlN* self-assembled quantum dots, *Rev. Mex. Fis.* **65** (2019) 231, https://doi.org/10.31349/revmexfis.65.231.
22. F. O. Oketch and H. O. Oyoko, A theoretical study of the effects of uniaxial stress and spatial dielectric functions on the density of states of shallow donor impurities in a *GaAs* quantum well dot of circular geometry, *Rev. Mex. Fis.* **70** (2024) 030501 1, https://doi.org/10.31349/RevMexFis.70.030501.
23. F. O. Oketch and H. O. Oyoko, A theoretical study of variation of photoionization cross section of donor impurities in a *GaAs* quantum dot of cylindrical geometry with incident photon frequency, donor location along the dot axis and applied uniaxial stress, *Rev. Mex. Fis.* **66** (2020) 35, https://doi.org/10.31349/revmexfis.66.35.
24. R. V. H. Hahn, F. Mora-Rey, R. L. Restrepo, A. L. Morales, J. Montoya-Sánchez, G. Eramo, M. G. Barseghyan, A. Ed-Dahmouny, J. A. Vinasco, D. A. Duque, and C. A. Duque, Electronic and optical properties of tetrapod quantum dots under applied electric and magnetic fields, *Eur. Phys. J. Plus* **139** (2024) 311, https://doi.org/10.1140/epjp/s13360-024-05089-z.
25. A. Manaselyan, M. G. Barseghyan, A. A. Kirakosyan, D. Laroze, and C. A. Duque, Effects of applied lateral electric field and hydrostatic pressure on the intraband optical transitions in a GaAs/$Ga_{1-x}Al_xAs$ quantum ring, *Physica E* **60** (2014) 95, https://doi.org/10.1016/j.physe.2014.02.015.
26. M. Sayrac, W. Belhadj, H. Dakhlaoui, and F. Ungan, Influence of structural variables and external perturbations on the nonlinear optical rectification, second, and third-harmonic generation in the *InP/InGaAs* triple quantum well structure, *Eur. Phys. J. Plus* **138** (2023) 1013, https://doi.org/10.1140/epjp/s13360-023-04630-w.
27. A. T. Tuzemen, E. B. Al, H. Dakhlaoui, and F. Ungan, Effects of external electric and magnetic field on the nonlinear optical rectification, second, and third-harmonic generations in *GaAs/AlGaAs* asymmetric triple quantum well, *Eur. Phys. J. Plus* **138** (2023) 668, https://doi.org/10.1140/epjp/s13360-023-04301-w.
28. M. B. Yücel, S. Sakiroglu, H. Sari, C. A. Duque, and E. Kasapoglu, Influence of external fields on the exciton binding energy and interband absorption in a double inverse parabolic quantum well, *Physica E* **144** (2022) 115433, https://doi.org/10.1016/j.physe.2022.115433.
29. E. Kasapoglu, M. B. Yücel, S. Sakiroglu, H. Sari, and C. A. Duque, Optical properties of cylindrical quantum dots with hyperbolic-type axial potential under applied electric field, *Nanomaterials* **12** (2022) 3367, https://doi.org/10.3390/nano12193367.
30. Z. Zeng, C. S. Garoufalis, and S. Baskoutas, Linear and nonlinear optical susceptibilities in a laterally coupled quantum-dot-quantum-ring system, *Phys. Lett. A* **378** (2014) 2713, https://doi.org/10.1016/j.physleta.2014.07.036.
31. A. Fakkahi, M. Kirak, M. Jaouane, A. Sali, A. Ed-Dahmouny, K. El-Bakkari, and R. Arraoui, The nonlinear optical rectification and second harmonic generation of a single electron confined in a multilayer spherical quantum dot, *Optical and Quantum Electron.* **55** (2023) 476, https://doi.org/10.1007/s11082-023-04730-y.
32. Y. Yakar, B. Çakır, C. Demir, and A. Özmen, Energy states, oscillator strengths and polarizabilities of many electron atoms confined by an impenetrable spherical cavity, *Int. J. Quantum Chem.* **121** (2021) e26658, https://doi.org/10.1002/qua.26658.
33. B. Vaseghi, M. Sadri, G. Rezaei, and A. Gharaati, Optical rectification and third harmonic generation of spherical quantum dots: Controlling via external factors, *Physica B* **457** (2015) 212, https://doi.org/10.1016/j.physb.2014.10.020.
34. B. Vaseghi, G Rezaei, and T Sajadi, Optical properties of parabolic quantum dots with dressed impurity: combined effects of pressure, temperature and laser intensity, *Physica B* **456** (2015) (2015) 171, https://doi.org/10.1016/j.physb.2014.08.034.
35. S. Taghipour, G. Rezaei, and A. Gharaati, Electromagnetically induced transparency in a spherical Gaussian quantum dot, *Eur. Phys. J. B* **95** (2022) 141, https://doi.org/10.1140/epjb/s10051-022-00409-7.
36. V. Ashrafi-Dalkhani, S. Ghajarpour-Nobandegani, and M. J. Karimi, Effects of spin-orbit interactions, external fields and eccentricity on the optical absorption of an elliptical quantum ring, *Eur. Phys. J. B* **92** (2019) 1, https://doi.org/10.1140/epjb/e2018-90691-5.
37. L. Máthé, C. P. Onyenegecha, A-A. Farcaş, L-M. Pioraş-Ţimbolmaş, M. Solaimani, and H. Hassanabadi, Linear and nonlinear optical properties in spherical quantum dots: Inversely quadratic Hellmann potential, *Phys. Lett. A* **397** (2021) 127262, https://doi.org/10.1016/j.physleta.2021.127262.
38. M. C. Onyeaju, J. O. A. Idiodi, A. N. Ikot, M. Solaimani, and H. Hassanabadi, Linear and nonlinear optical properties in spherical quantum dots: Manning-Rosen potential, *J. Optics* **46** (2017) 254, https://doi.org/10.1007/s12596-016-0359-9.
39. V. U. Unal, M. Tomak, and E. Aksahin, The effect of Coulomb interaction on optical absorption of a quantum well wire, Physica B **680** (2024) 415799, https://doi.org/10.1016/j.physb.2024.415799.
40. V. U. Unal, M. Tomak, E. Aksahin, and O. Zorlu, Nonlinear Optical Properties of Low Dimensional Quantum Systems in Progress in Nanoscale and Low-Dimensional Materials and Devices: Properties, Synthesis, Characterization, Modelling and Applications, (Springer, 2022) pp. 709-729. https://doi.org/10.1007/978-3-030-93460-6_25.

41. M. K. Bahar and P. Başer, The second, third harmonic generations and nonlinear optical rectification of the Mathieu quantum dot with the external electric, magnetic and laser field, *Physica Scripta* **665** (2023) 415042, https://doi.org/10.1016/j.physb.2023.415042.

42. A. E. Kavruk, M. Sahin, and Ü. Atav, A detailed investigation of electronic and intersubband optical properties of $Al_xGa_{1-x}As/Al_{0.3}Ga_{0.7}As/Al_y$ $Ga_{1-y}As/Al_{0.3}Ga_{0.7}As$ multi-shell quantum dots, *J. Phys. D:Appl. Phys.* **47** (2014) 295302, 10.1088/0022-3727/47/29/295302.

43. A. Haghighatzadeh, A. Attarzadeh, A. S. Durmuslar, E. B. Al, and F. Ungan, Modeling of electronic spectra and optical responses of a semiconductor AlGaAs/GaAs quantum well with three-step barriers: the role of external perturbations and impurity, *Eur. Phys. J. Plus* **139** (2024) 353, https://doi.org/10.1140/epjp/s13360-024-05165-4.

44. D. Makhlouf, M. Choubani, F. Saidi, and H. Maaref, Applied electric and magnetic fields effects on the nonlinear optical rectification and the carrier's transition lifetime in InAs/GaAs core/shell quantum dot, *Mater. Chem. Phys.* **267** (2021) 124660, https://doi.org/10.1016/j.matchemphys.2021.124660.

45. M. Servatkhah and R. Pourmand, Optical properties of a two-dimensional GaAs quantum dot under strain and magnetic field, *Eur. Phys. J. Plus* **135** (2020) 754, https://doi.org/10.1140/epjp/s13360-020-00773-2.

46. P. Hosseinpour, Kerr nonlinearity in asymmetric disc-like quantum dot and its controllability, *Physica B* **613** (2021) 412973, https://doi.org/10.1016/j.physb.2021.412973.

47. F. Rahimi, T. Ghaffary, Y. Naimi, and H. Khajehazad, Effect of magnetic field on energy states and optical properties of quantum dots and quantum antidots, *Optical and Quantum Electronics* **53** (2021) 1, https://doi.org/10.1007/s11082-020-02695-w.

48. K. A. Rodríguez-Magdaleno, F. M. Nava-Maldonado, E. Kasapoglu, M. E. Mora-Ramos, F. Ungan, and J. C. Martínez-Orozco, Nonlinear absorption coefficient and relative refractive index change for Konwent potential quantum well as a function of intense laser field effect, *Physica E* **148** (2023) 115618, https://doi.org/10.1016/j.physe.2022.115618.

49. N. Amin and A. J. Peter, Role of surrounding dielectric matrices on the nonlinear properties of group II-VI core/shell dot in the presence of electric field, *Micro and Nanostructures* **185** (2024) 207728, https://doi.org/10.1016/j.micrna.2023.207728.

50. E. B. Al, A. J. Peter, M. E. Mora-Ramos, and F. Ungan, Theoretical investigation of nonlinear optical properties of Mathieu quantum well, *Eur. Phys. J. Plus* **138** (2023) 49, https://doi.org/10.1140/epjp/s13360-023-03678-y.

51. Md. El-Yadri, J. El Hamdaoui, N. Aghoutane, L. M. Pérez, S. Baskoutas, D. Laroze, P. Díaz, and El. M. Feddi, Optoelectronic properties of a cylindrical core/shell nanowire: Effect of quantum confinement and magnetic field, *Nanomaterials* **13** (2023) 1334, https://doi.org/10.3390/nano13081334.

52. C. S. Garoufalis, D. B. Hayrapetyan, H. Sarkisyan, P. A. Mantashyan, Z. Zeng, I. Galanakis, G. Bester, T. Steenbock, and S. Baskoutas, Optical gain and entanglement through dielectric confinement and electric field in InP quantum dots, *Nanoscale* **16** (2024) 8447, https://doi.org/10.1039/D3NR06679G.

53. M. Choubani, H. Maaref, and F. Saidi, Linear, third-order nonlinear and total absorption coefficients of a coupled InAs/GaAs lens-shaped core/shell quantum dots in terahertz region, *Eur. Phys. J. Plus* **137** (2022) 265, https://doi.org/10.1140/epjp/s13360-022-02409-z.

54. R. L. Restrepo, E. Kasapoglu, S. Sakiroglu, F. Ungan, A. L. Morales, and C. A. Duque, Second and third harmonic generation associated to infrared transitions in a Morse quantum well under applied electric and magnetic fields, *Infrared Physics and Technology* **85** (2017) 147, https://doi.org/10.1016/j.infrared.2017.06.005.

55. U. Yesilgul *et al*., Linear and nonlinear optical properties in an asymmetric double quantum well under intense laser field: Effects of applied electric and magnetic fields, *Optical Materials* **58** (2016) 107, https://doi.org/10.1016/j.optmat.2016.03.043.

56. C. A. Duque, E. Kasapoglu, S. Sakiroglu, H. Sari, and I. Sökmen, Intense laser effects on donor impurity in a cylindrical single and vertically coupled quantum dots under combined effects of hydrostatic pressure and applied electric field, *Applied Surf. Sci.* **256** (2010) 7406, https://doi.org/10.1016/j.apsusc.2010.05.081.

57. R. Dutt, A. Mukherjee, and Y. P. Varshni, Dipole plarizability of hydrogen atom at high pressure, *Phys. Lett. A* **280** (2001) 318, https://doi.org/10.1016/S0375-9601(01)00067-6.

58. S. A. Ndengué, O. Motapon, R. L. M. Moleno, and A. J. Etindele, Electronic structure of a cylindrically confined hydrogen atom by the B-splines method: energy levels and dipole polarizability, *J. Phys. B: Atom. Mol. Opt.* **47** (2014) 015002, 10.1088/0953-4075/47/1/015002.

59. B. Çakir, Y. Yakar, and A. Özmen, Calculation of oscillator strength and the effects of electric field on energy states, static and dynamic polarizabilities of the confined hydrogen atom, *Optics Commun.* **311** (2013) 222, https://doi.org/10.1016/j.optcom.2013.08.015.

60. O. Motapon, S. A. Ndengué, and K. D. Sen, Static and dynamic dipole polarizabilities and electron density at origin: Ground and excited states of hydrogen atom confined in multiwalled fullerenes, *Int. J. Quantum. Chem.* **111** (2011) 4425, https://doi.org/10.1002/qua.22996.

61. X. Tian, C. Zhuang-Qi, O. Yong-Cheng, S. Qi-Shun, and Z. Guo-Long, Critical radius and dipole polarizability for a confined system, *Chinese Phys.* **15** (2006) 1172, https://doi.org/10.1088/1009-1963/15/6/008.

62. H. E. Montgomery, Dynamic dipole polarizabilities of the confined hydrogen atom, *Chem. Phys. Lett.* **352** (2002) 529, https://doi.org/10.1016/S0009-2614(01)01503-2.

63. S. Cohen, S. I. Themelis, and K. D. Sen, Dynamic dipole polarizabilities of the ground and excited states of confined hydrogen atom computed by means of a mapped Fourier grid method, *Int. J. Quantum. Chem.* **108** (2008) (2008) 351, https://doi.org/10.1002/qua.21459.

64. H. E. Montgomery Jr. and K. D. Sen, Dipole polarizabilities for a hydrogen atom confined in a penetrable sphere, *Phys. Lett. A* **376** (2012) 1992, https://doi.org/10.1016/j.physleta.2012.04.056.

65. S. Lumb, S. Lumb, and V. Prasad, Static polarizability of an atom confined in Gaussian potential, *Eur. Phys. J. Plus* **130** (2015) (2015) 149, https://doi.org/10.1140/epjp/i2015-15149-6.

66. N. M. Cann and A. J. Thakkar, Quadrupole oscillator strengths for the helium isoelectronic sequence: $n^1S - m^1D$, $n^3S - m^3D$, $n^1P - m^1P$, and $n^3P - m^3P$ transitions with $n < 7$ and $m < 7$, *J. Phys. B: At. Mol. Opt. Phys.* **35** (2002) 421, 10.1088/0953-4075/35/2/317.

67. Y. Yakar, B. Çakir, and A. Özmen, Dipole and quadrupole polarizabilities and oscillator strengths of spherical quantum dot, *Chem. Phys.* **513** (2018) 213, https://doi.org/10.1016/j.chemphys.2018.07.049.

68. A. Özmen, Y. Yakar, B. Çakir, and Ü. Atav, Computation of the oscillator strength and absorption coefficients for the intersubband transitions of the spherical quantum dot, *Optics Commun.* **282** (2009) 3999, https://doi.org/10.1016/j.optcom.2009.06.043.

69. L. J. Stevanović, Oscillator strengths of the transitions in a spherically confined hydrogen atom, *J. Phys. B: At. Mol. Opt. Phys.* **43** (2010) 165002, 10.1088/0953-4075/43/16/165002.

70. M. Das, Transition energies and polarizabilities of hydrogen like ions in plasma, *Physics of Plasmas* **19** (2012) 092707, https://doi.org/10.1063/1.4754716.

71. K. D. Sen, B. Mayer, P. C. Schmidt, J. Garza, R. Vargas, and A. Vela, Static dipole and quadrupole polarizability of confined hydrogen atom with $Z = N/3(N = 1 - 5)$, *Int. J. Quantum Chem.* **90** (2002) 491, https://doi.org/10.1002/qua.946.

72. W. H. Press, S. A. Teukolsky, W. T. Vetterling, and B. P. Flannery, Numerical Recipes in Fortran 77: The Art of Scientific Computing, 2nd Edn., Vol. 1 of Fortran Numerical Recipes (Press Syndicate of the University of Cambridge, 1997).